Study of transport, magnetic and magnetocaloric properties in Sr^{2+} substituted praseodymium manganite

Materials Research Express

PAPER

Study of transport, magnetic and magnetocaloric properties in Sr^{2+} substituted praseodymium manganite

Ajay Kumar Saw[1], **Ganesha Channagoudra**[1], **Shivakumar Hunagund**[2], **Ravi L Hadimani**[2] **and Vijaylakshmi Dayal**[1]

[1] Department of Physics, Maharaja Institutes of Technology Mysore, (VTU-Belagavi), 517477 India
[2] Department of Mechanical and Nuclear Engineering, Virginia Commonwealth University, 23285, United States of America

E-mail: drvldayal@gmail.com

Keywords: praseodymium strontium manganite ($PrSrMnO_3$), magnetoresistance, magnetic entropy

OPEN ACCESS

RECEIVED
15 October 2019

REVISED
12 December 2019

ACCEPTED FOR PUBLICATION
18 December 2019

PUBLISHED
6 January 2020

Abstract

The magnetotransport, magnetic and magnetocaloric properties in the polycrystalline $Pr_{1-x}Sr_xMnO_3$ ($0.20 \leqslant x \leqslant 0.40$) have been studied. The X-ray diffraction peaks for the composition $x = 0.20, 0.33$ and 0.40 have been indexed with orthorhombic structure having Pnma space group, whereas $x = 0.25$ composition has been indexed to *R*-3c space group having rhombohedral symmetry. The substitution of Sr^{2+} at Pr^{3+}site shows an increase in metal-insulator transition temperature (T_{MI}) and ferromagnetic ordering temperature (T_c). The composition, $x = 0.25$ shows the higher isothermal magnetic entropy change, $|\Delta S_m| = 2.84\ J\ kg^{-1}K^{-1}$ with RCP $= 116.33\ J\ kg^{-1}$ at $\Delta H = 3$ Tesla. The high RCP value ($=151.16\ J\ kg^{-1}$) with $|\Delta S_m| = 2.41\ J\ kg^{-1}\ K^{-1}$ at $\Delta H = 3$ Tesla for the composition, $x = 0.40$, implies that δT_{fwhm} plays a significant role.

1. Introduction

Perovskite manganites having common formula $R_{1-x}A_xMnO_3$ where 'R' is a rare-earth cation (La^{3+}, Pr^{3+}, Y^{3+}, Nd^{3+} etc) and 'A' an alkali or alkaline earth cation (Ca^{2+}, Sr^{2+}, Ba^{2+}, Na^{+}, K^{+}, etc) show a lot of interesting properties, arising from the strong interplay between spin, charge, orbital and lattice degrees of freedom [1–9]. Colossal magnetoresistance (CMR) phenomena observed in these manganites has been mainly explained through double exchange mechanism [10], phase separation [11] and spin-polarized tunnelling effect [12]. Besides the CMR properties, in the vicinity of ferromagnetic (FM) to paramagnetic transition temperature the manganites also show large magnetocaloric effect (MCE). These correlations of magneto-transport and magnetic properties in manganites make it suitable for a wide range of applications; such as in magnetic sensors, bolometric devices and magnetic refrigeration, which add to their multifunctionality and are studied continuously in recent years [12–18]. However, the prime challenge in these materials remains due to their complex transport and magnetic behaviour as well as study of the fundamental physics involved [1–4]. In this paper, we have discussed in detail the magnetotransport and magnetocaloric properties of $Pr_{1-x}Sr_xMnO_3$ ($0.20 \leqslant x \leqslant 0.40$) perovskite manganite.

2. Experimental

The polycrystalline $Pr_{1-x}Sr_xMnO_3$ ($0.20 \leqslant x \leqslant 0.40$) have been synthesized using the nitrate route. Powder of Pr_6O_{11}, $SrCo_3$ and MnO_2 were taken in stoichiometric ratio. The powders were ground and calcined several times between 800 °C and 1200 °C for 24 h with intermediate grindings. The powders thus, obtained were pressed into a pellet form at 10 MPa pressure and finally sintered at 1400 °C for 30 h with a cooling down to room temperature in air. The phase formation and structural characterization was carried out using powder x-ray diffraction (Bruker AXD-8 advance, CuKα radiation) at room temperature. DC electrical resistivity as a function of temperature and magnetic field down to 5 K was measured using the standard four-probe technique by means of resistivity/magnetoresistance set-up along with 8 T Oxford-Superconducting magnet at CSR,

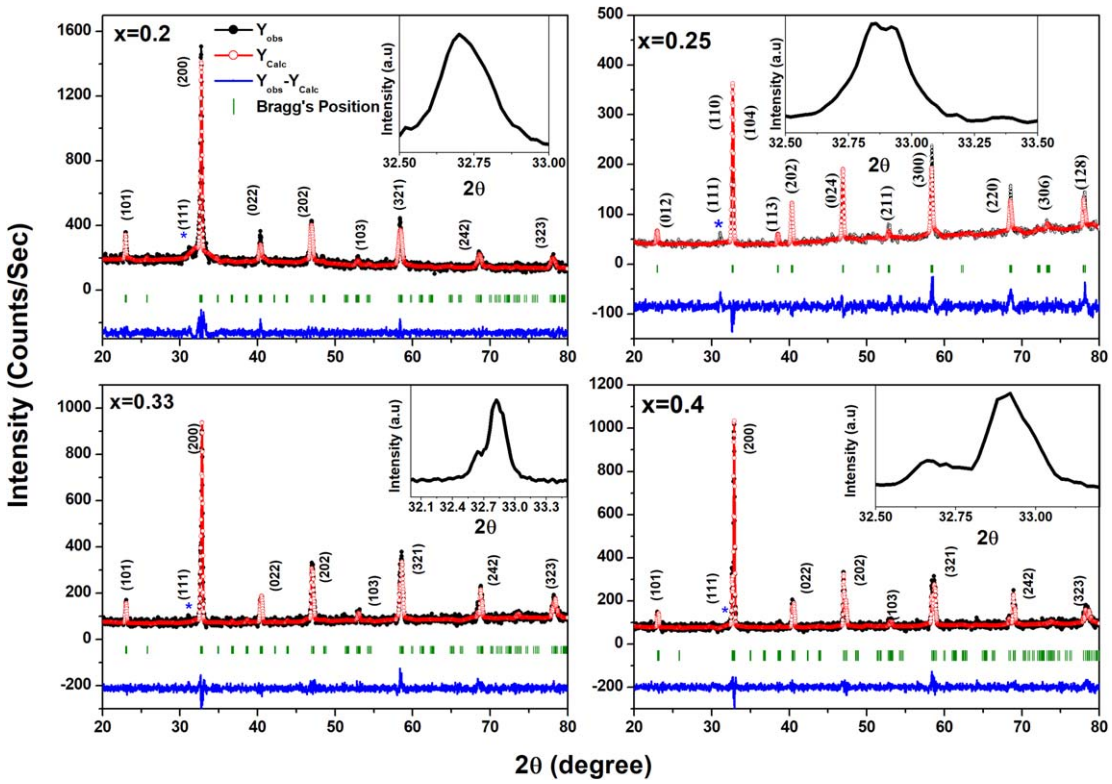

Figure 1. The x-ray diffraction patterns of $Pr_{1-x}Sr_xMnO_3$ ($0.20 \leqslant x \leqslant 0.40$) at room temperature along with Rietveld analysis. Inset shows highest intense peak in the XRD pattern for each composition.

Indore Centre. The magnetization (M) measurements as a function of temperature (T) and Magnetic field (H) were performed using Superconducting Vibrating Sample Magnetometer (VSM) (Versa Lab).

3. Result and discussion

3.1. Structural study

The x-ray diffraction (XRD) patterns of $Pr_{1-x}Sr_xMnO_3$ ($0.20 \leqslant x \leqslant 0.40$) along with Rietveld analysisof all the compositions carried out using Fullprof program are shown in the figure 1. We do not observe any impurity in this XRD pattern except for a very small and broad peak around $2\theta = 32°$, which could be due to a very small quantity Mn_5O_8 & Mn_3O_4 (111) phase. The intensity of this impurity peak in $x = 0.20$ composition is less than 1% of that of the (020) peak of highest intensity and weakens in later compositions. Similar results of the presence of impurity phase are reported in JCPDS-862337 and 22. The XRD pattern of $x = 0.20, 0.33$ and 0.40 compositions have been indexed to Pnma space group having orthorhombic symmetry, whereas, of $x = 0.25$ composition has been indexed to *R*-3c space group having rhombohedral symmetry. Inset of figure 1 shows highest intense peak in the XRD pattern for each composition.

The compositions with $x = 0.20, 0.33, 0.40$ having single intense peak and $x = 0.25$ having bifurcation in intense peak suggests the crystallization of their structure in orthorhombic and rhombohedral symmetry respectively in accordance with the Rietveld analysis. The relevant structural parameters obtained are tabulated in table 1. It has been observed that the unit cell parameter and cell volume decreases with increase in Sr^{2+} concentrations for $x = 0.20, 0.33$ and 0.40. It may be understood here that as Sr^{2+} (1.31 Å) has higher ionic radii of compared to Pr^{3+} (1.18 Å), hence generally the substitution may lead to increase in lattice parameter. The increase in the unit cell parameters and cell volume for $x = 0.25$ is understood due to its rhombohedral structure. Markovich *et al* [9], for $Pr_{1-x}Sr_xMnO_3$ single crystal (where, $x = 0.22, 0.24, 0.26$) also observed decrease in lattice parameter with increasing Sr^{2+} concentration and attributed it to a progressive decrease of Jahn–Teller distortions. Additionally, authors also suggested that for compositions with Sr^{2+} ($x > 0.3$), a structural transition to *R*-3c space group having rhombohedral symmetry must take place citing reference Boujelben *et al* [19].

Further, Knizek *et al* [20] in the composition range $0 < x < 0.5$ suggested the crystallization of compositions in orthorhombic symmetry having Pbnm space group and reported that the lattice volume decreases with increasing Sr^{2+} concentration. Chand *et al* [21], also reported the decrease in lattice parameter

Table 1. Lattice parameters obtained from Rietveld fittings to XRD pattern, Best fit values obtained from M(T) in PM region using CW law. MCE ΔS_M and RCP value.

$Pr_{1-x}Sr_xMnO_3$	x = 0.20	x = 0.25	x = 0.33	x = 0.40
a(Å)	5.459(9)	5.479 (7)	5.448(0)	5.442(3)
b(Å)	7.719(5)	5.479 (7)	7.701(4)	7.678(9)
c(Å)	5.493(3)	13.396(9)	5.482(1)	5.484(1)
V(Å^3)	231.533(1)	348.346(6)	230.013(4)	229.186(0)
T_{MI} (K)	100	200	253	230
(-)MR% at T_{MI} (8 T)	86	88	66	45
T_C (K)	150	186	261	286
C	0.0200	0.0199	0.0180	0.0171
θ_{CW}	160	190	236	268
μ_{eff}^{expt}	6.10	6.04	5.71	5.51
μ_{eff}^{cal}	4.90	4.64	4.25	3.95
$-\Delta S_M^{max}$ (J/kgK) (3 T)	…	2.84	2.36	2.41
δT_{fwhm} (K)	…	40.96	50.60	62.72
RCP (J/kg)(3 T)	..	116.33	119.42	151.16

with Sr^{2+} concentration x = 0.2, 0.3 and 0.5 in $Pr_{1-x}Sr_xMnO_3$. Nasari *et al* [22, 23] indexed the XRD pattern for $Pr_{0.6}Sr_{0.4}MnO_3$ having orthorhombic structure. Hence, the variation in lattice structures in our study are in accordance with the above discussed reported literature. The variation in structural parameters may be due to different method of preparation [7].

3.2. Magnetotransport study

The temperature dependent resistivity ρ(T) plot in the absence (0 T) and presence of magnetic field 5 T and 8 T are shown in figures 2(a)–(d). All the compositions show distinctive metal–insulator transition (T_{MI}), which increases for compositions with Sr^{2+}concentration x = 0.20–0.33 and decreases for x = 0.40. The decrease in resistivity and increase in T_{MI} indicates that with Sr^{2+} substitution, the ferromagnetic metallic state becomes more dominant. Additionally, the decrease in resistivity along with the increase in T_{MI} with the application of magnetic field also suggests the dominance of the magnetic field in enhancing the FM nature of the compositions. For lower composition x = 0.20, a large change in resistivity is observed around $T_{MI,}$ the metal to insulator transition becomes broader and shifted to a higher temperature side with the application of magnetic field as shown in figure 2(e). The temperature dependence of magnetoresistance, defined as $(MR)(\%) = \{([\rho(H) - \rho(0)]/\rho(0)) \times 100\}$ is also shown along with the resistivity curve in figures 1(a)–(d). Negative MR has been observed in the entire temperature range of measurement for all the compositions, however for compositions, x = 0.20 and 0.25, MR is nearly 80% around respective T_{MI} makes its suitable for the device application.

3.3. Magnetic properties study

The temperature dependent magnetization (T), of the compositions at 100 Oe down to 50 K is shown in the inset of figure 3. All the compositions show paramagnetic (PM) to ferromagnetic (FM) transition. Transition temperature T_C is determined from the minimum of dM/dT versus T curve. It can be observed that with the increase in Sr^{2+} concentration T_C increases significantly, from 150 K to 286 K, which clearly indicates the strengthening of ferromagnetism in accordance with the transport properties. As we increase Sr^{2+} (x), a lower saturation magnetization (M_S) is expected, as Sr is practically non-magnetic element. However, there is a crossover for M_S values between x = 0.20 and 0.25, breaks this systematic. As mentioned earlier in XRD section, x = 0.20 and 0.25 have orthorhombic and rhombohedral structural respectively. This structural transition may have lead to the increase in M_S value of x = 0.25 composition [19]. In order to understand the magnetic behavior of the compositions in the PM region above T_C, we studied the inverse of DC magnetic susceptibility (M/H) as a function of temperature (T) shown in figure 3. In high temperature region, much above T_C the DC magnetization data in paramagnetic region follows the Curie–Weiss (CW), expressed as $\chi = C/(T - \theta_{CW})$ as shown in figure 3.

Here C is a constant and can be defined as $C = b\mu_{eff}^2 N$, where μ_{eff} is the effective magnetic moment, 'b' is universal constant, 'N' is concentration of magnetic moments and θ_{CW} is the CW temperature. μ_{eff}^{expt} calculated from the linear fitting to the $\chi^{-1}(T)$ curves are tabulated in table 1 along with that expected from the theoretical model. The theoretical effective moment for each case can be written as $g\sqrt{s(s+1)}\ \mu_B$ for ($Mn^{3+}$and Mn^{4+}) and $g\sqrt{J(J+1)}\ \mu_B$ for $Pr^{3+}$where g is the gyromagnetic factor, S is the spin angular momentum, J(L ± S)is total angular momentum, L is orbital angular momentum and μ_B is the Bohr magneton. The theoretical values

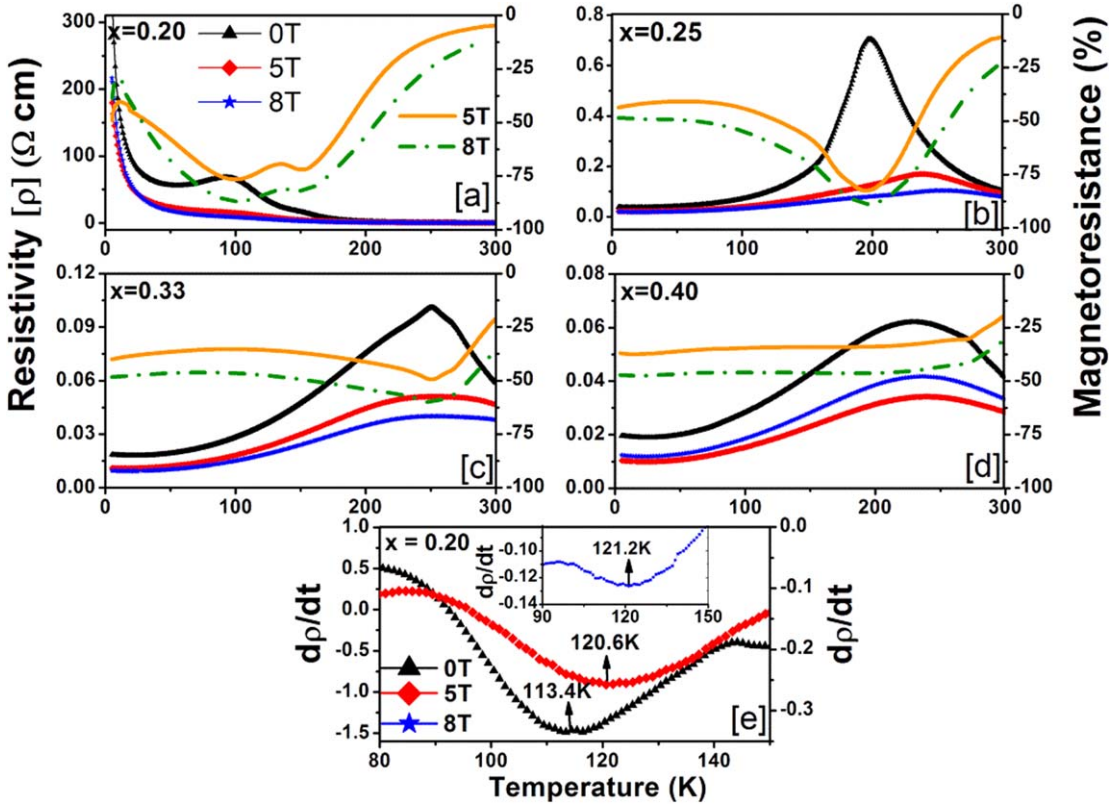

Figure 2. (a)–(d) Resistivity (ρ) versus Temperature (T) plots of the compositions measured at applied magnetic field of 0 T, 5 T and 8 T (Left). MR (%) versus T plots at 5 T and 8 T (Right). (e)dρ/dT versus T plot for x = 0.20 composition.

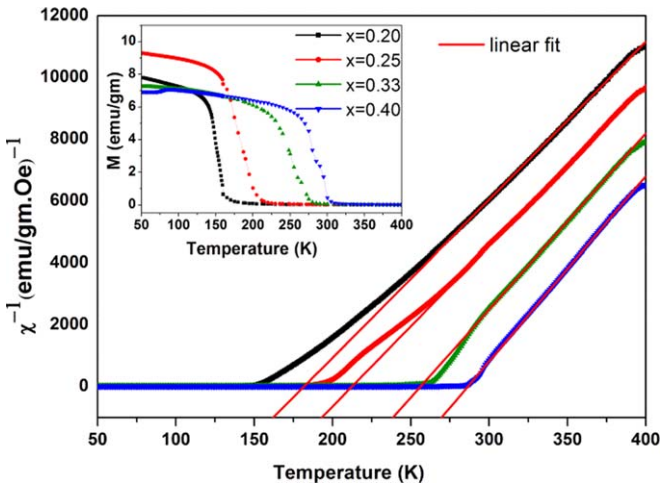

Figure 3. Inverse susceptibility versus T obtained from DC magnetization at 100 Oe DC. (Inset) Magnetization versus T plots.

of $\mu^{th}(Mn^{3+})$, $\mu^{th}(Mn^{4+})$ and Pr^{3+} are ~4.88μ_B, ~3.87μ_B and 3.58 μ_B respectively. The calculated μ_{eff}^{cal}/formula unit for the composition e.g. for x = 0.33 can be written as,

$$\mu_{eff}^{cal} = \sqrt{[(0.67)\mu_{eff}^{th}(Pr^{3+})\}]^2 + \{+[0.67\{\mu_{eff}^{th}(Mn^{3+}\}]^2 + [0.33\{\mu_{eff}^{th}(Mn^{4+})\}]^2}. \quad (1)$$

The C, θ_{CW}, μ_{eff}^{cal} and μ_{eff}^{expt} values so obtained from the best fit to the experimental data are listed in table 1. The obtained value of μ_{eff}^{exp} are found to be greater than that of μ_{eff}^{cal}. The difference between the experimental effective paramagnetic moment and the calculated can be explained by the existence of FM clusters within the PM phase, evidenced by the downturn in $\chi^{-1}(T)$ curve near T_C with the decreasing temperature [24, 25]. This downturn in $\chi^{-1}(T)$ suggests the deviation from CW law with the decreasing temperature and is an indication of non-analytical behaviour of magnetization arising from magnetic inhomogeneities [26–29].

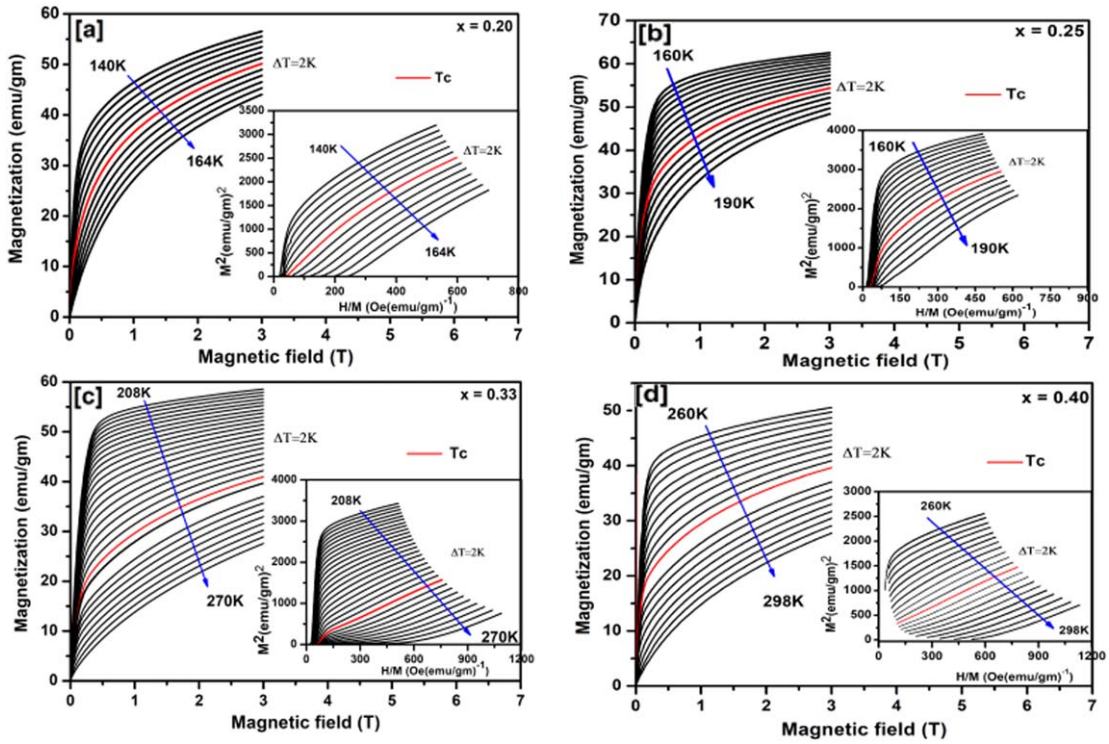

Figure 4. Dependence of magnetization on magnetic field at different temperatures. Inset displays the Arrott plots (M^2 versus H/M).

3.4. Magnetocaloric effect (MCE)

In order to study to the change in magnetic entropy (ΔS_M) with respect to the temperature (T), the magnetic field (H) dependent magnetizations (M) measured up to 3 T (within the instrumental limit) at the interval of 2 K and are shown in figures 4(a)–(d). As shown in the inset of figures 4(a)–(d), the observed positive slope for all studied temperatures specifies that the magnetic transition between the FM and PM phase is of the second order. The pragmatic second order transition without any thermal and magnetic hysteresis suggests that the compositions are suitable for refrigeration application. The magnetocaloric effect (MCE) is an intrinsic property of magnetic materials [30–36]. It is the heating or cooling of materials when subjected to magnetic field variation under adiabatic condition, which is maximized when the materials are near its magnetic ordering temperature.

Alternatively, MCE is also defined as isothermal change in entropy (ΔS_M) with change in magnetic field. The isothermal entropy change (ΔS_M) can be calculated from the isothermal magnetization curves. According to Maxwell′s thermo dynamical relations, the magnetic entropy change ΔS_M produced by the variation in a magnetic field from 0 to H_{max} is given by

$$\Delta S_M(T, H) = \int_0^H \left(\frac{\partial M}{\partial T}\right)_T dH \tag{2}$$

In case of magnetization measurement at small discrete fields and temperature intervals, numerical approximation to the integral could be expressed as

$$\Delta S_M(T, H) = \sum_i \frac{M_i - M_{i+1}}{T_i - T_{i+1}} \Delta H_i \tag{3}$$

where, $\Delta S_M = S_M(H, T) - \Delta S_M(0, T)$ is the magnetic entropy change, $M_{i+1}(T_{i+1}, H)$ and $M_i(T_i, H)$ are the magnetization values at temperature T_{i+1} and T_i, respectively, for a magnetic field interval of ΔH.

Figures 5(a)–(c) shows, $-\Delta S_M$ calculated using equation (2) for the compositions with x = 0.25, 0.33 and 0.40. The $-\Delta S_M$ value for x = 0.20 composition comparably less and hence not shown here. It can be observed that both the magnitude of $-\Delta S_M$ and its peak value $-\Delta S_M^{max}$, increases with the higher magnetic field change. It can be seen that, isothermal change in entropy (ΔS_m) is negative and shows caret like shape, which is typical of second order PM-FM transition in accordance with the Banerjee' criterion discussed earlier.

The magnetic isotherms measurements have been carried out with the difference of 2 K (ΔT), we have adopted a suitable fitting approach to obtain apparent maximum entropy change $-\Delta SM^{max}$ and full width at half maximum δT_{fwhm} and to further calculate relative cooling power (RCP). We used the Gaussian Asym equation, y = y0 + A × exp(−0.5((x − xc)/w)^2), where y0 is the offset, A denotes the amplitude, w is a

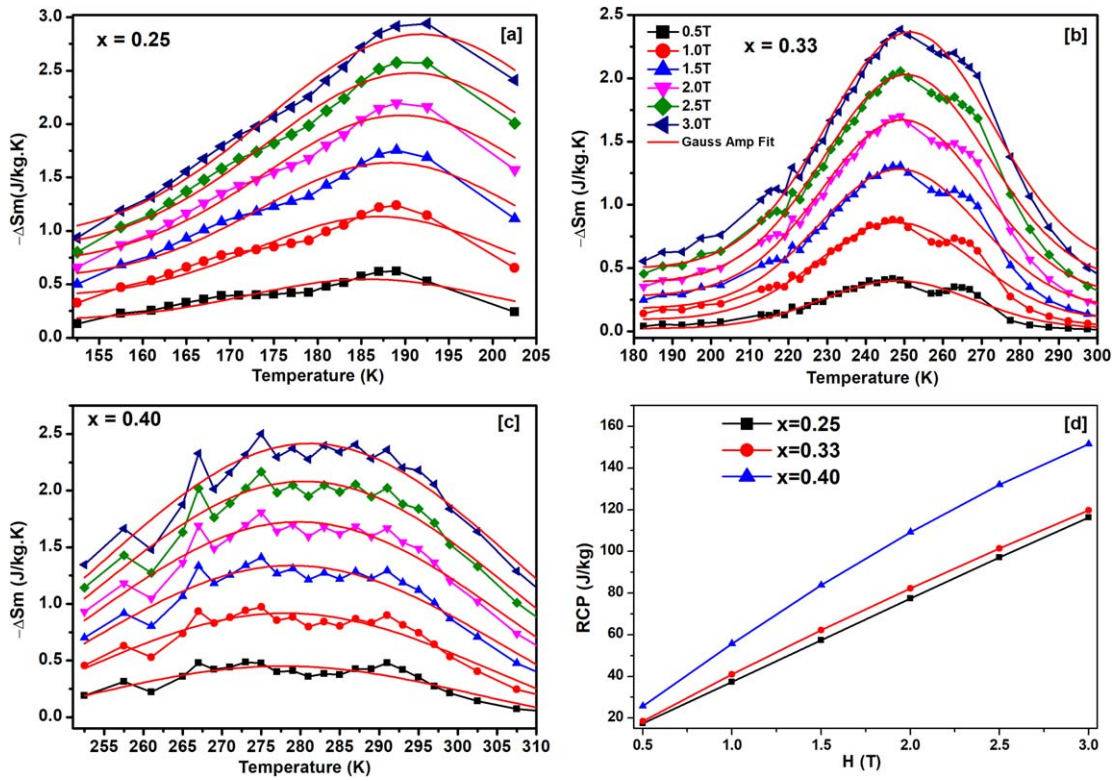

Figure 5. Magnetic entropy changes under applied fields ranging from 1 T to 3 T. (d) Displays the Relative Cooling Power plot.

Table 2. Reported Tc and ΔS value $Pr_{1-x}Sr_xMnO_3$ (x = 0.20 to 0.4) compositions synthesized by different methods and this work (in table 1).

Compositions	T_C (K)	ΔS_{max} (J/kg K)	Synthesized method	References
$Pr_{0.6}Sr_{0.4}MnO_3$	320	1.90	Solid state reaction	[14]
$Pr_{0.6}Sr_{0.4}MnO_3$	305	2.60	Solid state reaction	[15]
$Pr_{0.6}Sr_{0.4}MnO_3$	310	1.95	Solid state reaction	[16]
$Pr_{0.6}Sr_{0.4}MnO_3$	306	2.70	Solid state reaction	[17]
$Pr_{0.6}Sr_{0.4}MnO_3$	297	1.55	Solid state reaction	[22]
$Pr_{0.6}Sr_{0.4}MnO_3$	281	2.06	Ceramic Technology	[37]
$Pr_{0.6}Sr_{0.4}MnO_3$	295	2.90	Solid state reaction	[18]

parameter specifying the width called Gaussian width of the and xc represents the abscissa of the peak. Fitting $-\Delta S_M$ versus T plot with the said equation, the obtained best fit values (y0 + A) represents $-\Delta SM^{max}$ and $\delta T_{fwhm} = 2w \times \sqrt{(\ln 4)}$. The $-\Delta SM^{max}$, δT_{fwhm} and RCP values are tabulated in table 2. It can be observed that $-\Delta SM^{max}$ is maximum for x = 0.25 composition having value 2.84 J kg^{-1} K at 3 T. The relative cooling power (RCP), defined as $RCP = -\Delta SM^{max} \times \delta T_{fwhm}$, which provides a measure of the amount of heat transfer between hot and cold sinks during one ideal refrigeration cycle. The obtained RCP values of all the compositions are presented in figure 5(d). The higher RCP value 151.16 J kg^{-1} for x = 0.40 composition suggests that δT_{fwhm} plays a significant role.

4. Conclusions

Perovskite manganite $Pr_{1-x}Sr_xMnO_3$ with x = 0.20, 0.25, 0.33 and 0.40 are grown in single phase. The compositions x = 0.20, 0.33 and 0.40 crystallize in orthorhombic structure with Pnma space group, whereas x = 0.25 crystallize in Rhombohedra structure with $\overline{R}3c$ space group. Both metal to insulator transition and Curie temperature increases with increase in Sr^{2+} concentration. Magnetic measurements revealed that all the compositions undergo a second order magnetic transition with the PM–FM transition near room temperature. Through thermodynamic Maxwell relations, the isothermal entropy change ($-\Delta S_M$) has been determined. The entropy behaviour also suggests typical second order transition in all the studied compositions. The

compositions with Sr^{2+}concentration x = 0.25 and x = 0.40 shows a good magnetocaloric effect, indicating its potential application for refrigerant applications.

Acknowledgments

This work is supported by UGC DAE CSR, Indore (CSR-IC/CRS-89/2014-2018) and SERB-DST, New Delhi (EMR/2016/005424) grants. AKS (Project fellow II) gratefully acknowledges UGC DAE CSR and GC (JRF) SERB-DST for fellowship. Authors thank Dr Mukul Gupta and Layanta Behera for XRD measurements. We are grateful to Dr Rajeev Rawat and Sachin Kumar for resistivity/MR measurements at UGC-DAE Consortium for Scientific Research, Indore. Authors are thankful to Nanomaterials Core Characterization Facility (NCU) Virginia Commonwealth University, Richmond, USA for VSM facility.

ORCID iDs

Vijaylakshmi Dayal https://orcid.org/0000-0002-1330-0729

References

[1] Rao C N R and Raveau B (ed) 1998 *Colossal Magnetoresistance, Charge Ordering and Related Properties of Manganese Oxide* (Singapore: World scientific)
[2] Tokura Y (ed) 2000 *Colossal Magnetoresistance Oxides* (Singapore: Gordon and Breach)
[3] von Helmolt R, Wecker J, Holzapfel B, schulz L and Sammer K 1993 Giant negative magnetoresistance in perovskitelike La2/3Ba1/3MnOx ferromagnetic films *Phys. Rev. Lett.* **71** 2331
[4] Schiffer P, Ramirez A P, Bao W and Cheong S-W 1995 Low temperature magnetoresistance and the magnetic phase diagram of La1−xCaxMnO$_3$ *Phys. Rev. Lett.* **75** 3336
[5] Dayal V and Keshri S 2007 Structural and magnetic properties of $La_{0.67}Ca_{0.33}Mn_{1-x}Fe_xO_3$ (x = 0–0.07) *Solid State Commun.* **142** 63
[6] Kumar V P, Dayal Vijaylakshmi, Hadimani R L, Bhowmik R N and Jiles D C 2015 Magnetic and electrical properties of Ti-substituted lanthanum bismuth manganites *J. Mater. Sci.* **50** 3562–75
[7] Dayal V, Kumar P and Investigation V 2015 of complex magnetic state in $La_{0.8}Bi_{0.2}$MnO3 *J. Magn. Magn. Mater.* **361** 212–8
[8] Boujelben W, Ellouze M, Cheikhrouhou A, Cai Q, Pierre J, Yelon W B, Shimizu K and Dubourdieu C 2002 Neutron diffraction, NMR and magneto-transport properties in the Pr0.6 Sr0.4MnO3 perovskite manganite *J. of Alloys Compd.* **334** 1–8
[9] Markovich V, Fita I, Puziank R, Wisniewski A, Suzuki K, Cochrane J W, Yuzhelevskii Y, Mukovskii Y M and Gorodetsky G 2005 Pressure effects on the magnetic and transport properties of $Pr_{1-x}Sr_xMnO_3$ crystals near the percolation threshold *Phys. Rev. B* **71** 224409
[10] Zener C 1951 Interaction between the d-shells in the transition metals: II. Ferromagnetic compounds of manganese with perovskite structure *Phys. Rev.* **82** 403
[11] Dagotto E 2002 *Nanoscale Phase Separation and Colossal Magnetoresistanc* (Berlin Heidelberg New York: Springer)
[12] Hwang H Y, Cheong S-W, Ong N P and Batlogg B 1996 Spin-Polarized Intergrain Tunneling in La2/3Sr1/3MnO3 *Phys. Rev. Lett.* **77** 2041
[13] Gamatov A G, Batdalov A B, Aliev A M, Khurshilova Z, Elloouze M and Benjemma F 2017 Specific heat, thermal diffusion, thermal conductivity and magnetocaloric effect in $Pr_{0.6}Sr_{0.4}Mn_{1-x}FexO_3$ manganites *J. Magn. Magn. Mater.* **443** 352–7
[14] Zemni S, Baazaoui M, Dhahri J, Vincent H and Oumezzine M 2009 Above room temperature magnetocaloric effect in perovskite $Pr_{0.6}Sr_{0.4}MnO_3$ *Mater. Lett.* **63** 489–91
[15] Repaka D M, Tripathi T S, Aparnadevi M and Mahendiran R 2012 Magnetocaloric effect and magnetothermopower in the room temperature ferromagnet $Pr_{0.6}Sr_{0.4}MnO_3$ *J. Appl. Phys.* **112** 123915
[16] Thaljaoui R, Boujelben W, Pekala M, Pekala K, Fagnard J F, Vanderbemden P, Donten M and Cheikhrouhou A 2014 Magnetocaloric effect of monovalent K doped manganites $Pr_{0.6}Sr_{0.4-x}K_xMnO_3$ (x = 0 to 0.2) *J. Magn. Magn. Mater.* **352** 6–12
[17] Daivajna M D and Rao A 2016 Magnetocaloric effect in pristine and Bi-doped $Pr_{0.6}Sr_{0.4}MnO_3$ manganite *Solid State Commun.* **245** 65–9
[18] Rocco D L, Coelho A A, Gama S and de. Santos M 2013 Dependence of the magnetocaloric effect on the a-site ionic radius in isoelectronic manganites *J. Appl. Phys.* **113** 113907
[19] Boujelben W, Cheikh-Rouhou A, Ellouze M and Joubert J C 2000 Electrical properties in solid solution Pr_{1-x}SrxMnO3 (0 < x < 0.5) *Phys. Stat. Sol. (A)* **177** 503
Boujelben W, Cheikh-Rouhou A, Ellouze M and Joubert J C 2000 Synthesis, x-ray, magnetic and electrical studies of substituted (Pr, Sr)MnO_3 perovskites, *Phase Transitions: A Multinational Journal* **71** 127–41
[20] Knizek K, Jirak Z, Pollert E, Zounova F and Vratislav S 1992 Structure and magnetic properties of Pr1−xSrxMnO3 perovskites *J. of Solid State Chem.* **100** 292–300
[21] Chand U, Yadav K, Gaur A and Varma G D 2010 Structural, magnetic and magnetotransport properties of $Pr_{1-x}Sr_xMnO_3$ (x = 0.2, 0.3 & 0.5) synthesized by co-precipitation method *Optoelectronics and Adavanced materials-Rapid Commun.* **4** 1747–51
[22] Nasri A, Hlil E K, Lehlooh A-F, Ellouze M and Elhalouani F 2016 Study of magnetic transition and magnetic entropy changes of $Pr_{0.6}Sr_{0.4}MnO_3$ and $Pr_{0.6}Sr_{0.4}Mn_{0.9}Fe_{0.1}O_3$compounds *Eur. Phys. J. Plus* **131** 11
[23] Nasri A, Zouari S, Ellouze M, Rehspringer J L, Lehlooh A-F and Elhalouani F 2014 Structural and magnetic properties of $Pr_{0.6}Sr_{0.4}Mn_{1-x}Fe$ x O_3 ($0 \leqslant x \leqslant 0.3$) manganites oxide prepared by the ball milling method *J Supercond Nov Magn* **27** 443–51
[24] Martinez B, Laukhin V, Fontcuberta J, Pinsard L and Revcolevschi A 2002 Magnetic field and pressure effects on the magnetic transitions of $La_{0.9}Ca_{0.1}MnO_3$ perovskites *Phys. Rev. B: Condens. Matter Mater. Phys.* **66** 054436
[25] Banerjee B K 1964 On a generalized approach to first and second order magnetic transitions, on a generalized approach to first and second order magnetic transitions *Phys. Lett.* **12** 16–7
[26] Griffith's R B 1969 Nonanalytic behavior above the critical point in a random ising ferromagnet *Phys. Rev. Lett.* **23** 17

[27] Joshi L, Dayal V, Rama N and Keshri S 2009 Existence of Griffiths phase in $La_{0.67}Ca_{0.33}Mn_{0.93}Fe_{0.07}O_3$ *J. Alloys and Compd.* **479** 879–82
[28] Dayal V, Kumar V P, Hadimani R L and Jiles D C 2014 Evolution of Griffith's phase in $La_{0.4}Bi_{0.6}Mn1xTixO_3$ perovskite oxide *Journal of Applied Physics* **115** 17E111
[29] Pramanik A K and Banerjee A 2010 Griffiths phase and its evolution with Mn-site disorder in the half-doped manganite $Pr_{0.5}Sr_{0.5}Mn_{1-y}GayO_3$ (y = 0.0, 0.025, and 0.05) *Phys. Rev. B* **81** 024431
[30] Tishin A M and Spichkin Y I 2003 *The Magnetocaloric effect and its Applications* (Bristol: Institute of physics Publishing)
[31] Pecharsky V K and Gschneidner K A Jr 1997 Giant magnetocaloric effect in $Gd_5(Si_2Ge_2)$ *Phys. Rev. Lett.* **78** 4494
[32] Rawat R and Das I 2001 Magnetocaloric and magnetoresistance studies of $GdPd_2Si$ *J. of Phys: Condens Matt.* **12** L57
[33] Rawat R and Das I 2001 The similar dependence of the magnetocaloric effect and magnetoresistance in TmCu and TmAg compounds and its implications *J. of Phys: Condens Matt.* **19** L379
[34] Fu H, Hadimani R L, Ma Z, Wang M X, Teng B H and Jiles D C 2014 Magnetocaloric effect in $GdCo_xAl_{2-x}$ system for ($0.15 \leqslant x \leqslant 1$) compositions *J. of Appl. Phys* **115** 17A914 Magnetocaloric effect in GdCoxAl2−xsystem for ($0.15 \leqslant x \leqslant 1$) compositions
[35] Gutfleisch O, Willard M A, Bruck E, Chen C H, Sankar S G and Liu J P 2011 Magnetic materials and devices for the 21st century: stronger, lighter, and more energy efficient *Adv. Mater.* **23** 821
[36] Hamad M A and Theoretical J 2013 Therm. Theoretical work on magnetocaloric effect in ceramic and sol–gel $La_{0.67}Ca_{0.33}MnO_3$ *Anal. Calorim.* **111** 1251–4
[37] Gamzatov A G, Batdalov A B, Alieve A M, Ellouze M and Jemma F 2017 ISSN 1063–7834 *Physics of Solid State* **59** 2091–5